IEEE Access
Multidisciplinary | Rapid Review | Open Access Journal

Received May 20, 2019, accepted June 8, 2019, date of publication June 12, 2019, date of current version June 25, 2019.

Digital Object Identifier 10.1109/ACCESS.2019.2922173

Continuation Power Flow Model for Interconnected Systems Considering the Electricity Market Influence and Its Corresponding Distributed Algorithm

CHONG DING[1], (Student Member, IEEE), WEI YAN[1], (Member, IEEE), ZHOUYANG REN[1], (Member IEEE), RUIFENG ZHAO[2], WEI-JEN LEE[3], (Fellow, IEEE), AND XINYAN TANG[4]

[1]State Key Laboratory of Power Transmission Equipment & System Security and New Technology, Chongqing University, Chongqing 400044, China
[2]Power Dispatching Control Center, Guangdong Grid Company, China Southern Power Grid, Guangzhou 510600, China
[3]Energy Systems Research Center, University of Texas at Arlington, Arlington, TX 76013, USA
[4]Chongqing Snow Division, China Resources Group, Chongqing, Chongqing 400050, China

Corresponding author: Wei Yan (cquyanwei@cqu.edu.cn)

This work was supported in part by the National Natural Science Foundation of China, under Grant 51677012 and in part by the National "111" Project of China, under Grant B08036.

ABSTRACT The existing continuation power flow (CPF) methods, which mainly focus on regional independent systems, are not suitable for multi-area interconnected bulk systems in the electricity market environment. These existing CPF models cannot simulate the control behaviors of active/reactive power exchange among subsystems, and the corresponding CPF algorithms cannot satisfy the requirements of data sharing. This study presents a novel CPF model and its corresponding distributed algorithm for interconnected systems in which the influence of the electricity market is considered. This CPF method has the following unique features: 1) Regarding the bilateral power trading contracts (BPTCs) among regional subsystems, the nonlinear constraint equations of the directional trading active power via the interface are derived, and a multi-balancing machine strategy is introduced for realizing the active power balance of each subsystem. 2) Based on the simulation of the constant-voltage control behavior of the pilot buses in the regional automatic voltage control (AVC) system, the constant-voltage control behavior of the boundary buses of the tie-lines is further simulated to realize the reactive power balance among the regional subsystems. 3) According to the characteristics of the proposed CPF model, a novel distributed CPF algorithm based on block matrix computations is presented for realizing the decomposition and coordination calculation of multiple regional subsystems. This distributed algorithm preserves the precision and convergence of integrated CPF algorithms and has an advantage in terms of the calculation speed. The performance of the proposed CPF model and distributed algorithm is demonstrated via case studies and comparative analyses.

INDEX TERMS Automatic voltage control (AVC), bilateral power trading contract (BPTC), continuation power flow (CPF), distributed algorithm, interconnected bulk systems.

I. INTRODUCTION

The continuation power flow (CPF) method is an important and popular tool for the static voltage stability analysis of power systems [1]–[2]. However, all studies about CPF that have been reported in the literature mainly focus on regional independent systems and are not applicable to multi-area interconnected bulk systems under the electricity market environment.

Compared with regional independent systems, multi-area interconnected systems under the market environment impose special requirements on the active power exchange, reactive power exchange and data sharing among subsystems, which will introduce new challenges to the simulation of the power flow state and to the static voltage stability analysis of the interconnected systems.

The associate editor coordinating the review of this manuscript and approving it for publication was Guangdeng Zong.

(1) Special requirement on the active power exchange

In the electricity market environment, the directional trading active power (DTAP) transmitted between interconnected subsystems is determined according to the bilateral power trading contracts (BPTCs), and it cannot be changed during the contract period, even if the inner power flow of the subsystems varies [3]. This limitation represents an essential difference between the interconnected bulk systems and the independent regional grids. However, this issue is neglected in the existing literature on CPF. To simulate the active power distribution in the interconnected power systems accurately, the market constraint of constant active power exchange through the transmission interface between subsystems should be imposed in the CPF model.

(2) Special requirement on the reactive power exchange

Regional subsystems each have their own power-dispatching centres, which are required for realizing regional reactive power balance and for avoiding large amounts of reactive power exchange among subsystems. To accurately simulate the reactive power distribution of interconnected systems, it is necessary to model the reactive power control behaviour of the tie-lines in the CPF analysis.

(3) Special requirements on the distributed calculation and the confidentiality of commercial data

Under the market environment, the basic data of regional subsystems are of high commercial value, and commercial confidentiality is required in principle. Hence, it is essential to develop a multi-area distributed CPF algorithm that satisfies the requirement of basic data privacy. Furthermore, modern interconnected power systems are of a huge scale, with thousands of nodes. Improvement in the computational speed of the CPF algorithm for large-scale interconnected systems to satisfy the requirement of online static voltage stability analysis is another important problem that must be solved urgently.

However, the existing studies on CPF do not address the three problems discussed above. In this paper, a novel CPF model and its distributed algorithm are proposed for interconnected bulk systems, in which the influence of the electricity market is considered. First, in consideration of the influence of BPTC among regional subsystems, the nonlinear constraint equations of the directional trading active power (DTAP) via the interface are derived, and a multi-balancing machine strategy is introduced for realizing the active power balance of each subsystem. Second, based on the simulation of the constant-voltage control behaviour of pilot buses in the regional automatic voltage control (AVC) system, the constant-voltage control behaviour of the boundary buses of the tie-lines is further simulated in the proposed CPF model to realize reactive power balance among regional subsystems. Finally, a novel distributed CPF algorithm that is based on the block matrix computations is proposed for performing the decomposition and coordination calculations of multiple regional subsystems. The core method of this distributed algorithm is a special partitioning method for variables and equations, which is suitable for the characteristics of the proposed CPF model. With this partitioning method, the adjusted Jacobi matrix of the CPF model is of bordered block-diagonal form (BBDF), which facilitates parallel computation for solving the problems of data privacy and speed improvement in the CPF calculation for multi-area interconnected bulk systems. A two-area interconnected system that combines the IEEE 39-bus test system and the IEEE 118-bus test system was established, and many simulations and comparative analyses were conducted to evaluate the performance and validity of the proposed CPF model and the corresponding distributed algorithm.

The remainder of this paper is organized as follows: Section II reviews the CPF model for regional independent systems in which the influence of the AVC system is considered. Section III describes the proposed CPF model for interconnected systems in which the influence of the electricity market is considered. In Section IV, the proposed distributed CPF algorithm, which is based on block matrix computations, is described. A two-area interconnected system that combines the IEEE 39-bus test system and the IEEE 118-bus test system is used to demonstrate the proposed CPF model and the corresponding distributed algorithm in Section V. Finally, Section VI presents the conclusions of the paper.

II. CPF MODEL FOR THE REGIONAL INDEPENDENT SYSTEM UNDER THE INFLUENCE OF THE AVC SYSTEM

With the continuous improvement of automatic power-dispatching technology, the AVC system has become a core component of the provincial grid automatic dispatching system. According to the control schemes of the AVC system, each regional independent system will be divided into several control areas, and in each control area, various buses (namely, pilot buses) are selected to represent the overall voltage profiles [4]. The objective of the regional AVC system is to maintain the pilot buses at the reference voltages by controlling the reactive power output of a set of generating units (co-controlled generators) [5]. This control behaviour is referred to as the constant-voltage control of pilot buses [6].

Reference [7], presents a CPF model for the independent system in which the control characteristics of the AVC system are considered, and this CPF model has been widely proved effective. Compared with the conventional CPF model, this model has the following three differences: First, the bus types should be extended for simulating the constant-voltage control behaviours of pilot buses. Second, the coordinated equations of the reactive power outputs of P buses should be introduced when the control behaviour of the reactive power outputs of the co-controlled generators is considered. Finally, the parameterized power flow equations should be modified after the bus-types are extended. In addition to the above three differences, the step-size-constrained equation is constructed in the same way as the conventional CPF model. The modelling process of this CPF model is illustrated as follows:

(1) The bus-type extension

In this CPF model, in addition to the conventional PQ bus, PV bus and slack bus, the PQV bus and the P bus are introduced for simulating the constant-voltage control of pilot buses. The PQV bus models a pilot bus where not only the real and reactive power injection but also the magnitude of the voltage is assigned a priori. The P bus models a bus in which a co-controlled generator is connected. For the P bus, only the real power injection is assigned a priori.

(2) The extended parameterized power flow equations

After the new bus types have been defined, the extended parameterized power flow equations in which the AVC system is considered can be expressed as

$$\begin{cases} V_i \sum_{j\in i} V_j(G_{ij}\cos\theta_{ij} + B_{ij}\sin\theta_{ij}) - P_{gi}(\lambda) \\ \quad + (1+\lambda)\, P_{di0} = 0, \quad i \in \Omega_{PV}, \Omega_{PQ}, \Omega_{PQV}, \Omega_P \\ V_i \sum_{j\in i} V_j(G_{ij}\sin\theta_{ij} - B_{ij}\cos\theta_{ij}) \\ \quad + (1+\lambda)\, Q_{di0} = 0, \quad i \in \Omega_{PQ}, \Omega_{PQV} \end{cases} \tag{1}$$

where λ is the load growth factor; P_{di0} and Q_{di0} are the initial active and reactive loads, respectively, at bus i;$P_{gi}(\lambda)$ represents the parameterized active power output of generator bus i during load growth; and Ω_{PQV}, Ω_P, Ω_{PV} and Ω_{PQ} refer to the bus groups of PQV, P, PV and PQ buses, respectively.

Typically, the total active load increment is assumed to be distributed by generators according to the proportion of the residual active power capacity of each unit. Then, $P_{gi}(\lambda)$ in equation (1) can be expressed as

$$P_{gi}(\lambda) = P_{gi0} + \frac{P^i_{reserve}}{\sum_{i\in\Omega_g} P^i_{reserve}} \sum_{j\in\Omega_d} \lambda P_{dj0}, \quad i \in \Omega_g, \tag{2}$$

where P_{gi0} is the initial active power output of the generator at bus i; $P^i_{reserve}$ is the current residual active power capacity of the generator at bus i; Ω_d and Ω_g are the bus groups of load and generator buses, respectively; and P_{dj0} is the initial active load at bus j.

(3) The coordinated equations of the reactive power outputs of P buses

In the AVC system, the constant-voltage control of each PQV bus will be realized by controlling the reactive power output of co-controlled generators at a set of specified P buses. In this control relationship, each PQV bus corresponds to one P bus (one-to-one control) or multiple P buses (many-to-one control). If a PQV bus corresponds to multiple P buses, the coordination equations of the reactive power outputs of these P buses should be introduced into the CPF model. Assume that the reactive power output of the generators connected to these P buses is adjusted according to the proportion of the residual reactive power capacity of each unit. Then, the coordinated equations of the reactive power outputs of these P buses can be expressed as

$$\begin{cases} \dfrac{Q_{gi}(\lambda) - Q^{\min}_{gi}}{Q^{\max}_{gi} - Q^{\min}_{gi}} = \dfrac{Q_{gj}(\lambda) - Q^{\min}_{gj}}{Q^{\max}_{gj} - Q^{\min}_{gj}}, \quad i, j \in L_k,\ i \neq j \\ Q_{gi}(\lambda) = V_i \sum_{m\in i} V_m(G_{im}\sin\theta_{im} - B_{im}\cos\theta_{im}) \\ \qquad\qquad + (1+\lambda)\, Q_{di0} \end{cases} \tag{3}$$

where L_k refers to the group of P buses in the kth control area; $Q_{gi}(\lambda)$ and $Q_{gj}(\lambda)$ are the reactive power outputs of the ith and jth P buses in L_k, respectively; Q^{min}_{gi} and Q^{max}_{gi} are the upper and lower limits of the reactive power output of the ith P bus, respectively; and Q^{min}_{gj} and Q^{max}_{gj} are the upper and lower limits of the reactive power output of the jth P bus, respectively.

(4) The step-size-constrained equation

Parameterization is the key part of mathematical modelling, which directly affects the stability and the robustness of the CPF model. Choosing an appropriate parameterization method can overcome the singularity of Jacobian matrix at the saddle point and ensure the convergence of the CPF algorithm. The conventional parameterization methods include local [7], [8], arc-length [9], [10], and orthogonal parameterization [11]. The existing studies indicate that the orthogonal parameterization is not sensitive for some voltage instability cases with strong local characteristics, and it may lead to the non-convergence at the saddle point [12]. The local parameterization has good convergence. However, since the local parameterization adopts horizontal correction, the number of iterations is usually very large in the region with a small slope (e.g. the upper part of the PV curve). Given the quadratic characteristics of the parameterized equation and the large calculation residual, the PV curves can converge rapidly in the upper part of the curve, and diverging near the saddle point is difficult when the arc-length parameterization is used. The arc-length parameterization is selected in this study after comprehensive comparison with other parameterized methods. Then, the corresponding step-size-constrained equation can be expressed as

$$w(\boldsymbol{x}, \lambda) = (\boldsymbol{x} - \boldsymbol{x}^{prv})^T(\boldsymbol{x} - \boldsymbol{x}^{prv}) + (\lambda - \lambda^{prv})^2 - \sigma^2 = 0, \tag{4}$$

where $\boldsymbol{x}$ is the current state vector of all buses, which includes the voltage amplitudes and voltage phase angles; $\boldsymbol{x}^{prv}$ is the corresponding state vector at the previous operation point; λ and λ^{prv} are the load growth factors at the current and previous operation points, respectively; and σ refers to the step size.

Generally, equations (1), (3) and (4) form the CPF model for the regional independent system in which the influence of the AVC system is considered.

III. CPF MODEL FOR INTERCONNECTED SYSTEMS UNDER THE INFLUENCE OF THE ELECTRICITY MARKET

Based on the existing CPF model for regional independent systems, a novel CPF model for interconnected systems in which the influence of the electricity market is considered is

proposed in this Section. The proposed CPF model incorporates the following two innovations: First, the market constraint of constant active power exchanges among subsystems and its corresponding control behaviour are considered in the proposed CPF model. In consideration of the influence of BPTC among regional subsystems, the nonlinear constraint equations of DTPA via the interface are derived, and the multi-balancing machine strategy is introduced for realizing the active power balance of each subsystem. Second, the control behaviour for the partitioned reactive power balance in the multi-area interconnected systems is considered: In the proposed CPF model, based on the simulation of the constant-voltage control behaviour of the pilot buses, the constant-voltage control behaviour of the boundary buses of the tie-lines is further simulated to balance the partitioned reactive power and to avoid large amounts of reactive power exchange among subsystems.

A. NONLINEAR CONSTRAINT EQUATIONS OF DTAP VIA THE INTERFACE AND THE MULTI-BALANCING MACHINE STRATEGY

This paper considers a two-area interconnected system as an example for studying the influence of the BPTC on the active power exchanges among subsystems. A schematic diagram of a two-area interconnected system is shown in Fig. 1.

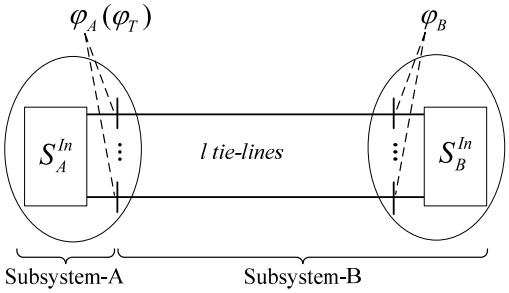

FIGURE 1. Schematic diagram of a two-area interconnected system.

In Fig. 1, φ_A denotes the boundary buses of the tie-lines in subsystem-A, and S_A^{In} denotes the interior buses in subsystem-A. Naturally, φ_A and S_A^{In} form the bus group of subsystem-A. Similarly, φ_B denotes the boundary buses of the tie-lines in subsystem-B, and S_B^{In} denotes the interior buses in subsystem-B. Together, φ_B and S_B^{In} form the bus group of subsystem-B. There is a transmission interface between subsystem-A and subsystem-B, which contains l AC tie-lines. As illustrated in Fig. 1, in the mathematical modelling of this paper, all these AC tie-lines are uniformly assigned to subsystem-B. Therefore, the common coupling bus between subsystem-A and subsystem-B, namely, φ_T, is actually equivalent to the boundary buses of the tie-lines in subsystem-A, namely, φ_A.

In the electricity market, bilateral active power contracts among regional subsystems are enforceable. The nonlinear constraint equations of DTAP via the interface can be expressed as

$$\begin{cases} \sum\limits_{\substack{j\in\varphi_A \\ k\in\varphi_B}} P_{jk}^{l} - P_{ref} = 0 \\ P_{jk}^{l} = V_j^2 \hat{G}_{jk} - V_j V_k (\hat{G}_{jk}\cos\theta_{jk} + \hat{B}_{jk}\sin\theta_{jk}) \end{cases} \tag{5}$$

where $\hat{G}_{jk}$ and $\hat{B}_{jk}$ are the conductance and the admittance of AC tie-line l_{jk}, respectively; and P_{ref} is the specified DTAP transmitted from subsystem-A to subsystem-B.

In a real power system, due to the unbalanced spatial and temporal distributions of the load and the power supply, the active power that is transmitted via the interface always varies with the load and power supply. When the load varies or increases in the interconnected systems, the active power output of the specific AGC unit in each subsystem should be adjusted to ensure that the total active power that is transmitted via the interface always satisfies the requirement of equation (5). Typically, one or more generators that have a quick regulating speed and large adjustable capacity are selected as the AGC units. The multi-balancing machine strategy is utilized in this study to simulate the controlling behaviours of AGC units. The implementation is described in detail as follows:

It is assumed that there is only one AGC unit in each subsystem, and the remaining generators are the planning units. Then, in each subsystem, the bus that connects to the AGC unit is defined as the active power balance bus, of which the voltage magnitude is specified. For example, there are two active power balance buses in the two-area interconnected system that is shown in Fig. 1. To guarantee the solvability of the power flow equations, one of the active power balance buses is selected as the voltage phase reference bus of the interconnected system. For distinction, the voltage phase reference bus is expressed as a Slack bus ($V\theta$ bus), and the remaining active power balance buses are expressed as Slack P buses (V bus). In other words, the Slack bus is set in one subsystem, of which the voltage magnitude and angle are specified. Simultaneously, a Slack P bus is set in every other subsystem, of which the voltage magnitude is specified.

B. CONTROL FOR THE PARTITIONED REACTIVE POWER BALANCE OF INTERCONNECTED SYSTEMS

Typically, there are multiple transmission tie-lines between subsystems, and the power allocation of the tie-lines is determined by the impedance of branches and power injections. If the load increases, the regional active power balance in each subsystem can be guaranteed by adjusting the active power outputs of the AGC units. However, due to the unbalanced distributions of the load and power supply, under the constraint of maintaining the total active power that is transmitted via the interface constant, the power allocation proportions of tie-lines will change substantially. In extreme scenarios, large overload or a severely unbalanced power distribution in tie-lines may occur [10]. The voltage amplitude deviations of the boundary buses of the tie-line may increase continuously, which will lead to large amounts of reactive

power transmission among regional subsystems. To satisfy the requirement of partitioned reactive power balance in each subsystem, an accurate simulation strategy for the constant-voltage control of boundary buses of tie-lines is proposed in this paper.

In terms of the mathematical modelling, the PQV bus and P bus model of the AVC systems in Section II can be adopted to realize the constant-voltage control of boundary buses. According to the control schemes of the AVC system, each subsystem will be divided into several control areas, and in each control area, several pilot buses will be selected to represent the overall voltage profiles. In this scenario, the PQV buses contain not only the pilot buses in each control area but also the boundary buses of the tie-lines in each subsystem. Compared with regional independent systems, the scope of PQV buses in the multi-area interconnected systems is expanded. Then, the partitioning result of the control areas should be redefined.

This study focuses on accurately simulating the control behaviour for the partitioned reactive power balance of the multi-area interconnected systems in the CPF model; the network partitioning method is not the focus or innovation of the proposed CPF model. The partitioning result of the control areas and the selection scheme for PQV buses and their associated co-controlled generator buses for an actual operating interconnected system are known in advance. Accordingly, this relevant information should be considered in the CPF calculation. However, the above information is incomplete for a standard test system. In this scenario, the partitioning result of control areas, the selection scheme for pilot buses and their associated co-controlled generator buses can be determined via the partitioning method in [13].

C. SUMMARY OF THE PROPOSED CPF MODEL

Equations (1)–(5) form the CPF model for interconnected systems in which the influence of the electricity market is considered. This model can be simply expressed as

$$\begin{cases} F(\boldsymbol{x}, \lambda) = 0 \\ S(\boldsymbol{x}, P_{ref}) = 0 \\ C(\boldsymbol{x}, \lambda) = 0 \\ w(\boldsymbol{x}, \lambda) = 0, \end{cases} \tag{6}$$

where $\boldsymbol{x}$ is the state vector of the AC buses, which includes the voltage amplitudes and voltage phase angles; $F(\bullet)$ represents the parameterized power flow equations after the scope of the PQV buses has been expanded, namely, equation (1); $S(\bullet)$ represents the constraint equation of DTAP via the interface, namely, equation (5); $C(\bullet)$ represents the coordinated equations of the reactive power output of the P buses, namely, equation (3); and $w(\bullet)$ represents the step-size-constrained equation, namely, equation (4).

The solvability of the proposed CPF model can be demonstrated by considering the two-area interconnected system in Fig. 1 as an example. For two-area interconnected systems, there is one Slack bus and one Slack P bus. The numbers of PQ buses, PV buses, PQV buses and P buses in the interconnected systems are denoted as n_{PQ}, n_{PV}, n_{PQV} and n_P, respectively. The following two scenarios can be analysed:

(1) When every PQV bus is in one-to-one control mode, namely, every PQV bus corresponds to only one P bus, then n_{PQV} equals n_P. Therefore, in the proposed CPF model, the number of active power flow constraint equations is $n_{PQV} + n_P + n_{PV} + n_{PQ}$, the number of the reactive power constraint equations is $n_{PQV} + n_{PQ}$, the number of the constraint equations of DTAP is 1, the number of coordinated equations of the reactive power output of the P buses is 0, and the number of step-size-constrained equations is 1. The CPF model has a total of $2n_{PQV} + n_P + n_{PV} + 2n_{PQ} + 2$ equations. In the unknown variables of the proposed CPF model, the number of voltage angles is $n_{PQV} + n_P + n_{PV} + n_{PQ} + 1$, and the number of voltage magnitudes is $n_{PQV} + n_{PQ}$. Furthermore, there is a load growth factor, namely, λ, in the unknown variables. Then, the CPF model has $2n_{PQV} + n_P + n_{PV} + 2n_{PQ} + 2$ variables. The number of equations is the same as the number of unknown variables, and the CPF model has a unique solution.

(2) When at least one PQV bus is operating in many-to-one control mode, namely, there are multiple co-generators that maintain constant the voltage amplitude of a same PQV bus, the following analysis can be performed: Assuming that a PQV bus corresponds to m_p P buses, then $m_p - 1$ reactive power constraint equations, $C(\bullet)$, and $m_p - 1$ unknown variables (voltage magnitudes) are added into the proposed CPF model. Therefore, the number of equations is the same as the number of unknown variables and the CPF model still has a unique solution.

During the load growth, when the voltage magnitudes or reactive power outputs of the P buses exceed the limits, the method in [5], [7] can be used to resolve these violation problems. The process is described in detail as follows:

(1) Exceeding the limits of the voltage magnitudes of P buses

If a P bus whose voltage magnitude exceeds the upper limit, namely, V_{max} (lower limit V_{min}), and its corresponding PQV bus are in one-to-one control mode, then this P bus will be converted to a PV bus, and its voltage magnitude will be set to V_{max} (V_{min}). At the same time, the corresponding PQV bus will be converted to a PQ bus.

If a P bus whose voltage magnitude exceeds the upper limit, namely, V_{max} (lower limit V_{min}), and its corresponding PQV bus are in many-to-one control mode, namely, this P bus and several other P buses jointly maintain constant the voltage magnitude of the corresponding PQV bus, then this P bus will be converted to a PV bus. The voltage magnitude of this PV bus will be set to V_{max} (V_{min}), and the bus types of the corresponding PQV bus and the other P buses in this control relationship will remain unchanged. As the load continues to increase, when all P buses in this many-to-one control relationship have exceeded the limits of the voltage

magnitudes and have been converted to PV buses, then the corresponding PQV bus will be converted to a PQ bus.

(2) Exceeding the limits of the reactive power output of P buses

If a P bus whose reactive power output exceeds the upper limit, namely, Q_{max} (lower limit Q_{min}), and its corresponding PQV bus are in one-to-one control mode, then this P bus will be converted to a PQ bus and its reactive power injection will be set as Q_{max} (Q_{min}). At the same time, the corresponding PQV bus will be converted to a PQ bus.

If a P bus whose reactive power output exceeds the upper limit, namely, Q_{max} (lower limit Q_{min}), and its corresponding PQV bus are in many-to-one control mode, the conversion process for the bus types differs from that described above. Because coordinated control for the reactive power output of the P buses has been adopted in the proposed CPF model, when the reactive power output of a P bus exceeds the upper limit (lower limit), the reactive outputs of all the other P buses in this many-to-one control relationship will also exceed the upper limit (lower limit) simultaneously. Therefore, all the P buses in this control relationship will be converted to PQ buses, and their reactive power injections will be set to the corresponding limit values. After all the P buses have been converted, the PQV bus will also be converted to a PQ bus.

IV. DISTRIBUTED CPF ALGORITHM BASED ON BLOCK MATRIX COMPUTATIONS

The existing distributed CPF algorithms for interconnected systems have various shortcomings. A distributed CPF algorithm that is based on the repeat power flow method is proposed in [14]. In this algorithm, the distributed computing process is only embodied in the solution of conventional power flow equations, and it cannot overcome the oscillation problem of the critical point in the repeated power method. Reference [15] presents a distributed CPF algorithm that is based on radial equivalent independent (REI)-type equivalents for multi-area power systems. This algorithm assumes that the interconnected systems can be divided into weak areas and non-weak areas of static voltage stability and that the ranges of these areas are known in advance. In the calculation flow, the REI equivalent networks of the non-weak areas are constructed. Then, the prediction-correction calculation is carried out by combining these equivalent networks with the weak areas to determine the load growth factor of the weak areas at the next operation point. Finally, the calculated load growth factor of the weak areas is directly used to modify the load level of the non-weak areas and update the load flow results. Via this approach, the distributed CPF is iterated repeatedly until the convergence condition is satisfied. However, this algorithm has the following shortcomings: The iterative value of the load growth factor in the weak areas is likely to be too large because its iterative calculation relies on the assumption that the REI-type equivalents remain approximately unchanged over a period of time, which may lead to non-convergence of the power flow near the critical point. Hence, a correction measure that halves the increment of the load growth factor in the case of non-convergence is also proposed in the above algorithm. Nevertheless, this correction measure is similar to the repeated power flow method, and it still cannot overcome the oscillation problem at the critical point.

For solving the non-convergence problem at the critical point of the existing distributed CPF algorithm, a novel distributed CPF algorithm that is based on block matrix computations is proposed for performing the decomposition and coordination calculations for multiple regional subsystems. The core component of this distributed algorithm is a special partitioning method for variables and equations that is suitable for the characteristics of the proposed CPF model. With this partitioning method, the adjusted Jacobi matrix of the CPF model is of bordered block-diagonal form (BBDF), which facilitates parallel computation for solving the problems of data privacy and speed improvement in the CPF calculation for multi-area interconnected bulk systems.

This paper will consider as an example the two-area interconnected system in Fig. 1 to demonstrate the calculation process of the proposed distributed algorithm, which can be easily extended to multi-area interconnected systems.

A. PARTITIONING METHOD FOR VARIABLES AND EQUATIONS IN THE PROPOSED CPF MODEL

The principles of the partitioning method that is used to partition the equations and variables should be discussed. Typically, the equations and variables in the power flow model can be partitioned directly via the partitioning of buses because regardless of whether it corresponds to a PQ, PV or Slack bus, the voltage vector is strongly related to its own power flow constraint equations. Except for the boundary buses that are related to two subsystems, each bus is only related to its own subsystem. Therefore, the boundary buses can be used as the coupling buses and the other buses as regional independent buses when the conventional power flow model is solved via the block computation method [16]–[19]. However, this partitioning method is not suitable for the proposed CPF model because the proposed CPF model differs from the conventional power flow model. The crucial differences are summarized as follows: First, in consideration of the bus types, the proposed CPF model not only contains the traditional PQ, PV and Slack buses but also the PQV, P and Slack $_{\mathrm{P}}$ buses. Second, in addition to the power flow constraint equations, the proposed CPF model contains the constraint equation of DTAP via the interface, coordinated equations of the reactive power output of the P buses and a step-size-constrained equation. Finally, in terms of the unknown variables, the proposed CPF model contains not only the voltage magnitudes and angles of the buses but also the public load growth factor λ of the interconnected systems.

According to the above characteristics of the proposed CPF model and the two-area interconnected power system that is illustrated in Fig. 1, the following partitioning strategies for equations and variables are developed in this paper:

1) As illustrated in Fig. 1, the two-area interconnected system is divided into subsystem-A and subsystem-B. All AC tie-lines are uniformly assigned to the subsystem where the Slack P is located, for example, the subsystem-B in Fig. 1. Recall that the common coupling bus between subsystem-A and subsystem-B, namely, φ_T, is equivalent to the boundary buses of the tie-lines in subsystem-A, namely, φ_A. Therefore, according to the proposed CPF model, as one of the boundary buses of the tie-lines, the common coupling bus, namely, φ_T, is also a PQV bus.
2) For PQ and PV buses, the power flow constraint equations and their voltage variables (magnitudes and angles) are assigned to the subsystems where these buses are located.
3) For the PQV buses (excluding φ_T) and their associated P buses, the power flow constraint equations, the coordinated equations of the reactive power output of these P buses and their voltage variables are assigned to the subsystems where these buses are located.
4) For φ_T and its associated P buses, the power flow constraint equations of φ_T and the coordinated equations of the reactive power output of these P buses are assigned to the coupling equations, and the voltage angle of φ_T and the voltage magnitudes of these P buses are assigned to the unknown coupling variables. The active power constraint equations and the voltage angles of these P buses are still assigned to the subsystems where they are located.
5) For the Slack P bus, because all AC tie-lines between subsystems have been uniformly divided into subsystem-B, the constraint equation of DTAP via the interface and the voltage angle of the Slack P bus are assigned to subsystem-B.
6) The load growth factor, namely, λ, is related to all subsystems. Therefore, λ is assigned to the unknown coupling variables, and the step-size-constrained equation is assigned to the coupling equations.

Based on the above strategies, the partitioning schemes for the variables and equations of the proposed CPF model can be described in detail as follows:

(1) The partitioning scheme for subsystem-A

The variables and equations of subsystem-A are divided into two parts:

Part-I corresponds to the variables and equations that are associated with the interior buses of subsystem-A. This part includes the following:

① the voltage magnitudes and angles of the PQ buses in subsystem-A and their active and reactive power constraint equations;

② the voltage angles and the active power constraint equations of the PV buses in subsystem-A;

③ the voltage angles of the PQV buses (excluding φ_T) in subsystem-A and their active and reactive power constraint equations; and

④ the voltage magnitudes and angles of the P buses that are associated with the PQV buses (excluding φ_T), the active power constraint equations of these P buses and the coordinated equations of the reactive power output of these P buses.

Part-II corresponds to the variables and equations that are associated with the common coupling bus φ_T. This part includes the voltage angles of the P buses that are associated with φ_T and the active power constraint equations of these P buses.

(2) The partitioning scheme for subsystem-B

The variables and equations of subsystem-B are also divided into two parts. The first part corresponds to the variables and equations that are associated with the interior buses of subsystem-B. The composition of this part is the same as that of Part-I of subsystem-A. The second part corresponds to the variables and equations that are related to the tie-lines, which includes the constraint equation of DTAP via the interface and the voltage angle of the Slack P bus.

(3) The partitioning scheme for the coupling zone

The variables and equations of the coupling zone include the following:

① the voltage angles and the power constraint equations of φ_T;

② the voltage magnitudes of the P buses that are associated with φ_T and the coordinated equations of the reactive power output of these P buses; and

③ the load growth factor, namely, λ, and the step-size-constrained equation.

Combined with the above partitioning scheme, the proposed CPF model, namely, equation (6), can be expressed as the following block structure:

$$\begin{cases} \boldsymbol{y}_A(\boldsymbol{x}_A, \boldsymbol{x}_T) = 0 \\ \boldsymbol{y}_B(\boldsymbol{x}_B, \boldsymbol{x}_T) = 0 \\ \boldsymbol{y}_T(\boldsymbol{x}_A, \boldsymbol{x}_B, \boldsymbol{x}_T) = 0, \end{cases} \tag{7}$$

where $\boldsymbol{y}_A$, $\boldsymbol{y}_B$ and $\boldsymbol{y}_T$ represent the equations of subsystem-A, subsystem-B and the coupling zone, respectively, and $\boldsymbol{x}_A$, $\boldsymbol{x}_B$ and $\boldsymbol{x}_T$ represent the unknown variables of subsystem-A, subsystem-B and the coupling zone, respectively.

The unknown partitioning variables, namely, $\boldsymbol{x}_A$, $\boldsymbol{x}_B$ and $\boldsymbol{x}_T$, can be expressed in sequence as

$$\begin{cases} \boldsymbol{x}_A = [\theta_A, V_A] \\ \boldsymbol{x}_B = [\theta_B, V_B] \\ \boldsymbol{x}_T = [\theta_T, V_P^{\varphi}, \lambda], \end{cases} \tag{8}$$

where θ_A and V_A refer to unknown voltage angles and magnitudes, respectively, in subsystem-A; θ_B and V_B refer to unknown voltage angles and magnitudes, respectively, in subsystem-B; θ_T refers to the voltage angle of φ_T; V_P^{φ} refers to the voltage magnitudes of the P buses that are associated with φ_T; and λ refers to the load growth factor.

Similarly, the partitioning equations, namely, $\boldsymbol{y}_A$, $\boldsymbol{y}_B$ and $\boldsymbol{y}_T$, can be expressed in sequence as

$$\begin{cases} \boldsymbol{y}_A = \{F_A(\boldsymbol{x}_A, \boldsymbol{x}_T); C_A(\boldsymbol{x}_A, \boldsymbol{x}_T)\} \\ \boldsymbol{y}_B = \{F_B(\boldsymbol{x}_B, \boldsymbol{x}_T); C_B(\boldsymbol{x}_B, \boldsymbol{x}_T); S(\boldsymbol{x}_B, \boldsymbol{x}_T)\} \\ \boldsymbol{y}_T = \{F_T(\boldsymbol{x}_A, \boldsymbol{x}_B, \boldsymbol{x}_T); C_T(\boldsymbol{x}_A, \boldsymbol{x}_B, \boldsymbol{x}_T); w(\boldsymbol{x}_A, \boldsymbol{x}_B, \boldsymbol{x}_T)\}, \end{cases} \tag{9}$$

where $F_A(\bullet)$, $F_B(\bullet)$ and $F_T(\bullet)$ refer to the active and reactive power constraint equations in subsystem-A, subsystem-B and the coupling zone, respectively; $C_A(\bullet)$, $C_B(\bullet)$ and $C_T(\bullet)$ refer to the coordinated equations of the reactive power output of the P buses in subsystem-A, subsystem-B and the coupling zone, respectively; and $S(\bullet)$ and $w(\bullet)$ are as defined in equation (6).

B. BLOCK CALCULATION FOR THE PREDICTION STEP

The conventional CPF process consists of four basic steps: parameterization, prediction, correction, and step-length control [20]. The calculation is dominated by the prediction step and the correction step.

Once a basic solution has been identified (for $\lambda = 0$), the next solution can be predicted by taking an appropriately sized step in a direction tangent to the solution path. By applying the tangent method [21] to the CPF model for multi-area interconnected systems in the block structure, namely, equation (7), the prediction equation can be expressed as

$$\begin{bmatrix} J_{AA} & 0 & J_{AT} \\ 0 & J_{BB} & J_{BT} \\ J_{TA} & J_{TB} & J_{TT} \end{bmatrix} \begin{bmatrix} d\boldsymbol{x}_A \\ d\boldsymbol{x}_B \\ d\boldsymbol{x}_T \end{bmatrix} = \begin{bmatrix} 0 \\ 0 \\ e \end{bmatrix} \tag{10}$$

where $e = [0, \ldots, 0, \pm 1]^T$ and the length of e is equal to the number of equations in $\boldsymbol{y}_T$; $[d\boldsymbol{x}_A, d\boldsymbol{x}_B, d\boldsymbol{x}_T]$ is the tangent vector of unknown variables; and J represents the matrix of the partial derivatives.

The matrix of the partial derivatives, namely, J, can be expressed as

$$\begin{cases} J_{ii} = \dfrac{\partial \boldsymbol{y}_i}{\partial \boldsymbol{x}_i}, & i = \text{A, B} \\ J_{iT} = \dfrac{\partial \boldsymbol{y}_i}{\partial \boldsymbol{x}_T}, & i = \text{A, B} \\ J_{Ti} = \dfrac{\partial \boldsymbol{y}_T}{\partial \boldsymbol{x}_i}, & i = \text{A, B} \\ J_{TT} = \dfrac{\partial \boldsymbol{y}_T}{\partial \boldsymbol{x}_T}. \end{cases} \tag{11}$$

The coefficient matrix of equation (10) is of bordered block-diagonal form (BBDF) [18], [22], and all diagonal submatrices of it are invertible square matrices. Via the strictly equivalent linear transformation, the prediction equation (10) can be transformed to the following decoupling equations:

$$(-\sum\nolimits_{i=A,B} J_{Ti} J_{ii}^{-1} J_{iT} + J_{TT}) d\boldsymbol{x}_T = e \tag{12}$$

$$d\boldsymbol{x}_i = -J_{ii}^{-1} J_{iT} d\boldsymbol{x}_T, \quad i = A, B \tag{13}$$

By calculating equations (12) and (13) in turn, the tangent vector $[d\boldsymbol{x}_A, d\boldsymbol{x}_B, d\boldsymbol{x}_T]$ can be obtained. Then, the prediction will be computed as

$$\begin{cases} \boldsymbol{x}_i^* = \boldsymbol{x}_i^{m-1} + \sigma d\boldsymbol{x}_i, & i = A, B \\ \boldsymbol{x}_T^* = \boldsymbol{x}_T^{m-1} + \sigma d\boldsymbol{x}_T, \end{cases} \tag{14}$$

where superscript $*$ denotes the predicted solution at the present operation point, superscript $m-1$ denotes the corrected solution at the previous operation point, and σ is a scalar value that is used to adjust the step size.

The data that are required for calculating the coefficient submatrices in equations (12) and (13) are discussed below to ensure parallel computations. According to the detailed expressions of the proposed CPF model, for the ith subsystem (i = A, B), only the local information (model data and variable state data) is needed for calculating partial derivatives J_{ii}, J_{iT} and J_{Ti}. Therefore, these partial derivatives can be calculated independently by the regional server of each subsystem. Submatrix J_{TT} is related to all subsystems, however, the calculation of its elements is regionally independent. When calculating the elements that correspond to the coupling buses and their associated P buses in the ith subsystem (i = A, B), only the local information of the ith subsystem and the state data of the coupling variables are needed. Hence, each subsystem can independently calculate submatrix $J_{TT}^{(i)}$ (i = A, B) with the same dimension and upload it to the central coordinated server. Then, the central server can directly calculate J_{TT} via the following equation:

$$J_{TT} = \sum\nolimits_{i=A,B} J_{TT}^{(i)}. \tag{15}$$

The block calculation flow for the prediction step is summarized as follows:

P-Step 1: The central coordinated server sends the impedance parameters of the tie-lines and the current state values of the coupling variables $\boldsymbol{x}_\text{T}$ to each regional server.

P-Step 2: Based on the regional model data, the regional state data and the current values of $\boldsymbol{x}_\text{T}$, the regional server calculates coefficient matrices $J_{Ti}J_{ii}^{-1}J_{iT}$ and $J_{TT}^{(i)}$ (i = A, B). Then, these coefficient matrices will be sent to the central coordinated server.

P-Step 3: In combination with the coefficient matrices that are uploaded by the regional servers, the central coordinated server will calculate J_{TT} via equation (15) and calculate $d\boldsymbol{x}_T$ via equation (12). After the calculations have been completed, $d\boldsymbol{x}_T$ will be sent to the regional servers.

P-Step 4: According to $d\boldsymbol{x}_T$, each regional server calculates $d\boldsymbol{x}_i$ (i = A, B) independently via equation (13).

P-Step 5: Based on equation (14), the central server calculates the predicted solution of coupling variables $\boldsymbol{x}_T^*$ iteratively and saves it, while each regional server calculates the predicted solution of regional variables $\boldsymbol{x}_i^*$ (i = A, B) independently and saves it.

C. BLOCK CALCULATION FOR THE CORRECTION STEP

The predicted solutions, namely, $\boldsymbol{x}_i^*$ and $\boldsymbol{x}_T^*$, will be regarded as the initial values of the proposed CPF model in the block structure. The Newton-Raphson algorithm is used for

iterative calculation until convergence. The Taylor series is used to express equation (7) and the second- and higher-order terms are neglected. The corresponding correction equation can be expressed as

$$\begin{bmatrix} J_{AA} & 0 & J_{AT} \\ 0 & J_{BB} & J_{BT} \\ J_{TA} & J_{TB} & J_{TT} \end{bmatrix} \begin{bmatrix} \Delta \boldsymbol{x}_A \\ \Delta \boldsymbol{x}_B \\ \Delta \boldsymbol{x}_T \end{bmatrix} = - \begin{bmatrix} \Delta \boldsymbol{y}_A \\ \Delta \boldsymbol{y}_B \\ \Delta \boldsymbol{y}_T \end{bmatrix} \tag{16}$$

where $\Delta \boldsymbol{x}_i$ (i = A, B) and $\Delta \boldsymbol{x}_T$ are the deviations of the variables of the ith subsystem and the coupling zone, respectively, and $\Delta \boldsymbol{y}_i$ (i = A, B) and $\Delta \boldsymbol{y}_T$ are the unbalanced quantities of the equations of the ith subsystem and the coupling zone, respectively. The meanings of partial derivatives J_{ii}, J_{iT}, J_{Ti} and J_{TT} (i = A, B) are the same as those in equation (10). The correction equation (16) has the same BBDF structure as the prediction equation (10) because the coefficient matrices of these two equations are identical.

Via the strictly equivalent linear transformation, the correction equation (16) can be transformed to

$$(-\sum_{i=A,B} J_{Ti} J_{ii}^{-1} J_{iT} + J_{TT}) \Delta \boldsymbol{x}_T = -\Delta \boldsymbol{y}_T + \sum_{i=A,B} J_{Ti} J_{ii}^{-1} \Delta \boldsymbol{y}_i \tag{17}$$

$$\Delta \boldsymbol{x}_i = -J_{ii}^{-1} J_{iT} \Delta \boldsymbol{x}_T - J_{ii}^{-1} \Delta \boldsymbol{y}_i, \quad i = A, B \tag{18}$$

The data that are required for calculating the coefficient submatrices in equations (17) and (18) are discussed below to ensure parallel computations. Referring to the analysis above, the partial derivatives J_{ii}, J_{iT}, J_{Ti}, and J_{TT} (i = A, B) and the unbalanced quantities $\Delta \boldsymbol{y}_i$ (i = A, B) can be calculated independently by the regional servers with the local information. Similar to the calculation of J_{TT}, the unbalanced quantity of the coupling equations, namely, $\Delta \boldsymbol{y}_T$, is related to all subsystems; however, the calculation of its elements is regionally independent. Therefore, each subsystem can independently calculate submatrix $\Delta \boldsymbol{y}_T^{(i)}$ (i = A, B) with the same dimension and upload it to the central coordinated server. Then, the central server can directly calculate $\Delta \boldsymbol{y}_T$ via the following equation:

$$\Delta \boldsymbol{y}_T = \sum\nolimits_{i=A,B} \Delta \boldsymbol{y}_T^{(i)} \tag{19}$$

The block calculation flow for the correction step is summarized as follows:

C-Step 1: Each server accepts the predicted solutions $\boldsymbol{x}_i^*$ (i = A, B) and $\boldsymbol{x}_T^*$ and regards them as the initial values of the correction calculation.

C-Step 2: The central coordinated server sends the current values of the coupling variables $\boldsymbol{x}_\mathrm{T}$ to every regional server. Based on the regional model data, the state data and the current value of $\boldsymbol{x}_\mathrm{T}$, the regional server calculates coefficient matrices $J_{Ti} J_{ii}^{-1} J_{iT}$, $J_{Ti} J_{ii}^{-1} \Delta \boldsymbol{y}_i$, $J_{TT}^{(i)}$ and $\Delta \boldsymbol{y}_T^{(i)}$. Then, these matrices will be sent to the central coordinated server.

C-Step 3: Combined with the coefficient matrices that were uploaded by the regional servers, the central coordinated server will calculate J_{TT} and $\Delta \boldsymbol{y}_T$ via equations (15) and (19), respectively, and calculate the iterative quantity of the coupling variables, namely, $\Delta \boldsymbol{x}_T$, via equation (17). After the calculation has been completed, $\Delta \boldsymbol{x}_T$ will be sent to the regional servers.

C-Step 4: Each regional server accepts $\Delta \boldsymbol{x}_T$ and calculates $\Delta \boldsymbol{x}_i$ (i = A, B) independently via equation (18).

C-Step 5: The central coordinated server updates the coupling variables $\boldsymbol{x}_T$ with the iterative quantity $\Delta \boldsymbol{x}_T$, and each regional server updates the variables of each subsystem $\boldsymbol{x}_i$ with $\Delta \boldsymbol{x}_i$. After all the variables have been updated, the regional servers and the central coordinated server will calculate the unbalanced quantities of the equations of each subsystem and the coupling zone, namely, $\Delta \boldsymbol{y}_i$ and $\Delta \boldsymbol{y}_T$, respectively.

C-Step 6: The calculation convergence criterion for the correction step is evaluated. If $max(\|\Delta \boldsymbol{y}_A\|, \|\Delta \boldsymbol{y}_B\|, \|\Delta \boldsymbol{y}_T\|) < 10^{-6}$, then the present correction step has converged, the current values of variables $\boldsymbol{x}_i$ (i = A, B) and $\boldsymbol{x}_T$ are saved as the corrected solution, and the CPF calculation proceeds to the next prediction step. If the convergence criterion of the correction step is not satisfied, then the algorithm returns to C-Step 2.

D. STEP CONTROL AND THE CONVERGENCE CRITERION

Non-saddle point failure is the other type of the computation failures in CPF calculation. Choosing an appropriate variable-step-size algorithm can avoid the phenomenon of divergence at non-saddle point [12]. The variable-step-size algorithm in [23] is widely used to overcome the non-saddle point failure. Since this algorithm is well documented in the literature, it will not be detailed here.

The variable-step-size algorithm in [23] is adopted in this paper, and the convergence criterion of the proposed distributed CPF algorithm is

$$\lambda^m < \lambda^{m-1} \tag{20}$$

where λ^m and λ^{m-1} refer to the load growth factors that are calculated at the current operation point and the previous operation point, respectively.

E. CPF CALCULATION FLOW

See Fig. 2.

F. DISCUSSION OF THE COMPUTATIONAL ACCURACY, CALCULATION SPEED, COMMUNICATION TRAFFIC AND COMMERCIAL CONFIDENTIALITY

The proposed distributed CPF algorithm, which is based on block matrix computations, has similarities in the prediction step and the correction step. In this part, the correction step is considered as an example to identify the characteristics of the proposed algorithm in terms of the computational accuracy, calculation speed, communication traffic and commercial confidentiality.

According to comprehensive observations of the block calculation flow of the correction step, the distributed algorithm

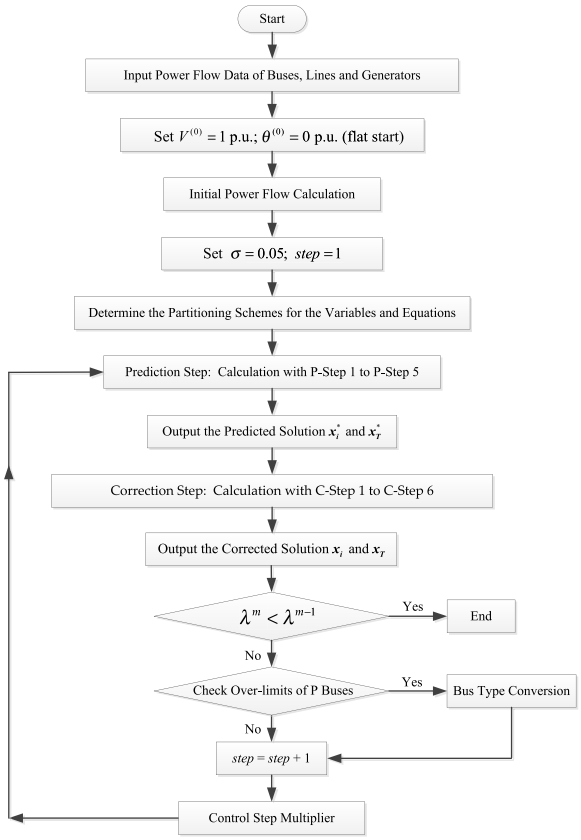

FIGURE 2. Calculation flow of the proposed distributed CPF algorithm.

that is proposed in this paper is equivalent to transforming the centralized calculation of equation (16) into the serial block calculation of equations (17) and (18) and the regional parallel block calculation of equation (18). Because there is no approximation in this equivalent transformation, the proposed distributed algorithm has very high computational accuracy.

Compared with the original centralized coefficient matrix in equation (16), the sizes of the partitioning matrices in equations (17) and (18) are greatly reduced. In addition, iterative computation is not necessary in the serial block calculation or the parallel block calculation. Therefore, the proposed distributed CPF algorithm has an advantage in terms of the calculation speed according to a comparison with the integrated algorithms.

Regarding the communication traffic, the coupling variables of the proposed distributed algorithm are only the voltage angles of the boundary buses, the load growth factor λ, and the voltage magnitudes of the P buses that are associated with the boundary buses. The number of coupling variables is very small; it typically ranges from a few to a dozen. Therefore, the proposed distributed algorithm encounters no difficulties regarding the information communication among subsystems.

Finally, throughout the entire calculation process, only a small amount of data needs to be transferred between the central coordinated server and the regional servers, and no commercial data need to be transferred among the regional servers. Hence, the proposed algorithm can also satisfy the commercial confidentiality requirements for the internal data of regional power grid companies.

V. CASE STUDIES

The results of case studies and a comparative analysis on a two-area interconnected system that combines the IEEE 39-bus test system and the IEEE 118-bus test system demonstrate the high performance of the proposed CPF model and the corresponding distributed method.

A. TEST DATA AND SIMULATION SCHEMES

Figure 3 shows a single-line diagram of the two-area interconnected system. The entire test system is divided into two subsystems, namely, subsystem-A and subsystem-B. Based on the original case data, two AC tie-lines (A9–B9 and A22–B81) are added as the transmission interface between the subsystems. The following BPTC is assumed: An active power of 400 MW must be transferred from subsystem-B to subsystem-A directionally via the transmission interface. The impedance information of the AC tie-lines is listed in Table 1.

TABLE 1. Impedance information of ac tie-lines.

Line	Resistance (p.u.)	Reactance (p.u.)	Susceptance (p.u.)
L1 (A9-B9)	0.0057	0.0625	1.0290
L2 (A22-B81)	0.0057	0.0625	1.0290

As shown in Fig. 3, to simulate the control effect of the AVC system, subsystem-A and subsystem-B are each divided into three electrical control areas. The relationships between the PQV buses and their associated P buses in each control area are presented in Table 2.

TABLE 2. Relationships between pqv buses and p buses.

Subsystem	Control Area	Ω^i_{PQV}	Ω^i_P
Subsystem-A	AVC A1	bus-A26	bus-A30, bus-A37, bus-A38
	AVC A2	bus-A9	bus-A39
		bus-A12	bus-A32
	AVC A3	bus-A16	bus-A33, bus-A34
		bus-A22	bus-A35, bus-A36
Subsystem-B	AVC B1	bus-B9	bus-B8, bus-B10
		bus-B23	bus-B25
	AVC B2	bus-B50	bus-B49
		bus-B81	bus-B80
	AVC B3	bus-B96	bus-B100

To facilitate the analysis of the influences of BPTC in the electricity market and the constant-voltage control behaviour of the boundary buses of the tie-lines on the voltage stability margin (VSM) and to identify the calculation characteristics of the proposed distributed algorithm, the following schemes are simulated:

Scheme M1: The proposed CPF model and its distributed algorithm are adopted. The nonlinear constraint equation of

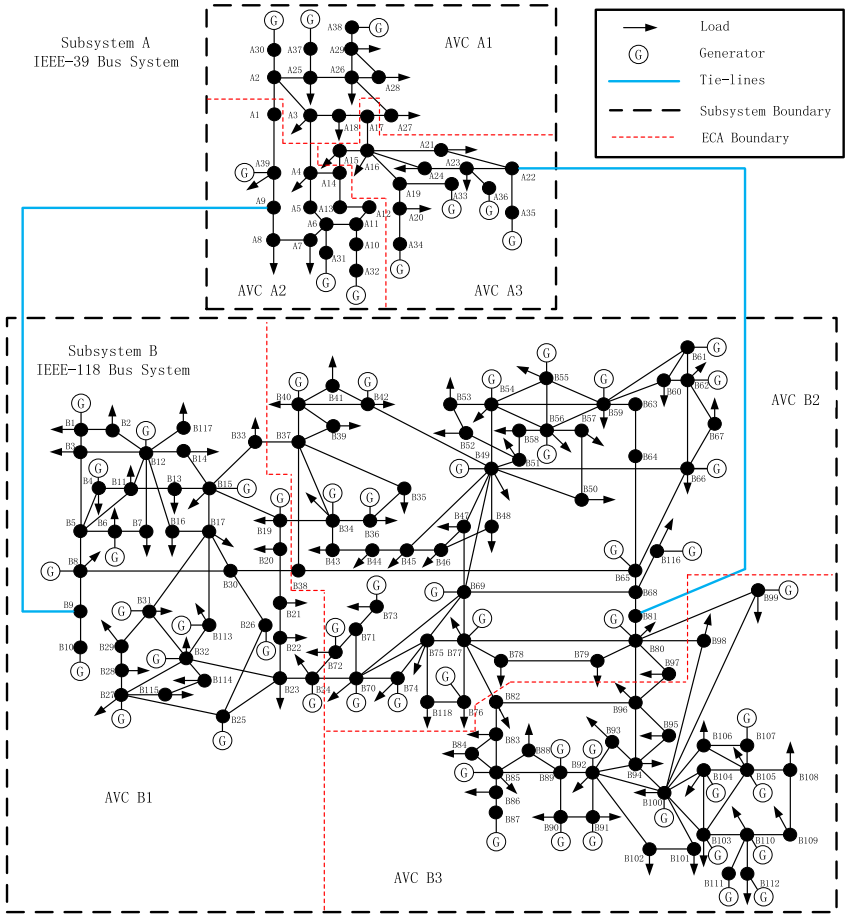

FIGURE 3. Two-area interconnected system that combines the IEEE 39-bus test system and the IEEE 118-bus test system.

DTAP that is derived from BPTC is considered. The constant-voltage control behaviour of the boundary buses of the tie-lines is further simulated to realize the reactive power balance among the regional subsystems. In the end, the algorithm is developed and implemented in MATLAB.

Scheme M2: This scheme is identical to scheme M1 except it does not simulate the constant-voltage control behaviour of the boundary buses of tie-lines.

Scheme M3: This scheme is identical to scheme M1 except it does not adopt the distributed algorithm. Instead, the proposed CPF model is solved via a typical integrated algorithm [21].

Scheme M4: All subsystems are simulated independently while ignoring BPTC. The tie-lines are assumed to be equivalent to the constant loads at the boundary buses of the subsystems, and the equivalent loads can be calculated from the initial power flow. The CPF model for regional independent systems that is presented in Section II is adopted.

B. INFLUENCE OF BPTC ON VSM

The influence of BPTC on the VSM in the CPF calculation can be observed by comparing simulation schemes M2 and M4. The only difference between schemes M2 and M4 is that the nonlinear constraint equation of DTAP that is derived from BPTC is considered in scheme M2. In the CPF, the critical load growth factor λ_{max}, which refers to the ratio of the maximum additional load increment to the initial load, is commonly used to characterize the VSM. The calculated VSMs under schemes M2 and M4 are listed in Table 3.

TABLE 3. VSMs under schemes M2 and M4.

Scheme	VSM (λ_{max})
M2	0.3204
M4	0.7797 (subsystem-A) 0.8360 (subsystem-B)

As listed in Table 3, the VSM under scheme M2 is 0.3204, whereas the VSMs under scheme M4 are 0.7797 (subsystem-A) and 0.8360 (subsystem-B). The VSMs of M4 are more than twice as large as that of M2. Hence, the VSM result will deviate greatly from the real value when the CPF model that is based on the PQ equivalent method is applied.

Fig. 4 shows the curves of the transmission power in AC tie-lines L1 and L2 under scheme M2. L1 refers to

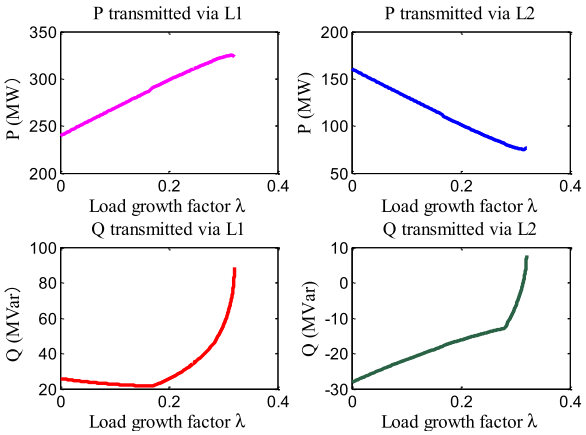

FIGURE 4. Curves of the transmission power in tie-lines under scheme M2.

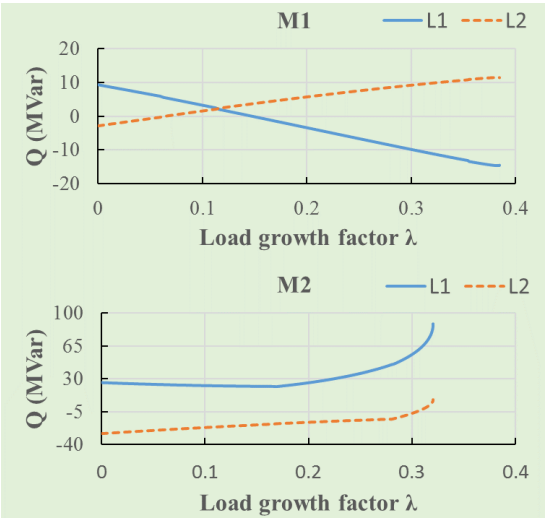

FIGURE 5. Curves of the transmission reactive power in tie-lines under schemes M1 and M2.

line A9-B9, whereas L2 refers to line A22-B81. If the power value is positive, then the power direction is from bus B9 to bus A9 or from bus B81 to bus A22. As shown in Fig. 4, as the load increases, the active power transmitted in L1 increases from 239.57 MW to 323.32 MW, and the reactive power transmitted in L1 initially decreases from 25.75 MVar to 21.46 MVar and subsequently gradually increases to 88.52 MVar. The active power transmitted in L2 decreases from 160.43 MW to 76.68 MW, and the reactive power transmitted increases from −28.16 MVar to 7.74 MVar. With the introduction of BPTC, when the load increases, the active power allocation proportion and reactive power transmitted in tie-lines will undergo a dramatic change. Thus, the VSM under scheme M2 differs from that under scheme M4.

C. INFLUENCE OF THE CONSTANT-VOLTAGE CONTROL BEHAVIOUR OF BOUNDARY BUSES ON VSM

The influence of the constant-voltage control behaviour of the boundary buses of tie-lines on the VSM can be demonstrated by comparing schemes M1 and M2. The VSMs that are calculated under schemes M1 and M2 are listed in Table 4 below. The VSM of scheme M1 is 0.3846, whereas that of scheme M2 is 0.3204; the former is 1.20 times the latter. This difference shows that whether the constant-voltage control of boundary buses is considered or not has a substantial influence on the VSM of the interconnected systems.

TABLE 4. VSMs under schemes M1 and M2.

Scheme	VSM (λ_{max})
M1	0.3846
M2	0.3204

Fig. 5 shows the curves of the reactive power transmitted in the tie-lines under schemes M1 and M2. As shown in Fig. 5, for scheme M1, the reactive power transmitted in L1 decreases from 9.41 MVar to −14.62 MVar and that transmitted in L2 increases from −2.91 MVar to 11.43 MVar.

The maximum fluctuations of the reactive power transmitted in L1 and L2 are 24.03 MVar and 14.34 MVar, respectively. Similarly, for scheme M2, the reactive power transmitted in L1 initially decreases from 25.75 MVar to 21.46 MVar and subsequently, rapidly increases to 88.82 MVar, while the reactive power transmitted in L2 increases from −28.16 MVar to 7.74 MVar. The maximum fluctuations of the reactive power transmitted in L1 and L2 under scheme M2 are 67.36 MVar and 35.9 MVar, respectively. According to the simulation comparison, ignoring the constant-voltage control of the boundary buses of tie-lines (in M2) may lead to many reactive power exchanges among subsystems in the process of load growth. In contrast, considering the constant-voltage control of boundary buses (in M1) can not only ensure the reactive power balance among the regional subsystems but also improve the VSM of the interconnected systems substantially.

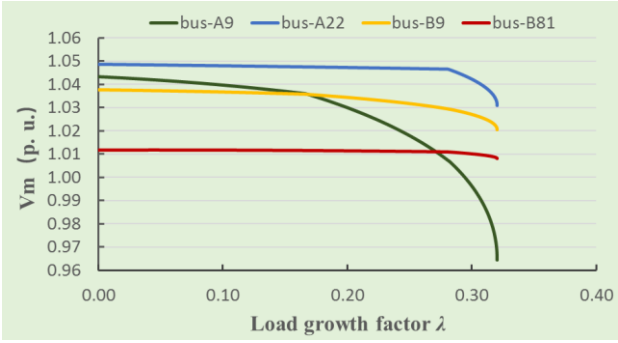

FIGURE 6. V–λ curves of the boundary buses of tie-lines under M2.

Fig. 6 shows the V–λ curves of the boundary buses of tie-lines under scheme M2. The voltage magnitudes of the boundary buses decrease substantially, especially those of bus-A9 and bus-A22. The fluctuations in the voltage magnitudes of boundary buses may cause the voltage magnitude difference between the terminals of the tie-line to

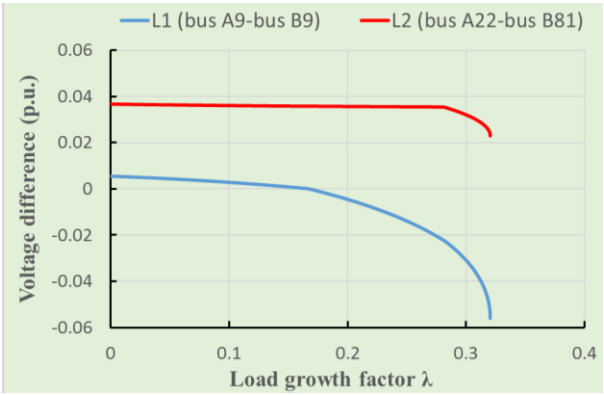

(a)

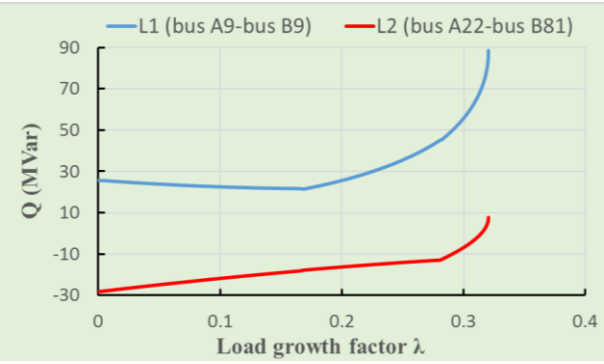

(b)

FIGURE 7. (a) Curves of the voltage magnitude differences between both terminals of tie-lines under M2. (b) Curves of the transmission active power in tie-lines under M2.

fluctuate substantially; then, large amounts of reactive power would be transmitted between subsystems.

The curves of the voltage magnitude differences between the terminals of tie-lines and the curves of the transmission active power in tie-lines under scheme M2 are shown in Fig. 7. According to Fig. 7, the voltage magnitude difference between the terminals of tie-line L1 initially decreases from 0.0054 p.u. to zero and subsequently increases to −0.0562 p.u. Correspondingly, the active power transmitted in L1 initially decreases from 25.75 MVar to 21.46 MVar and subsequently increases to 88.52 MVar. The amount of reactive power transmitted in tie-lines is strongly correlated with the voltage magnitude difference between the terminals of tie-lines. Therefore, by considering the constant-voltage control of boundary buses, it is possible to avoid many of the reactive power exchanges among subsystems.

Table 5 lists the detailed exit information of the AVC control strategies under schemes M1 and M2. In Table 5, the exit point refers to the load growth factor when the exit operation of the AVC control strategy occurs; exit-PQV bus Ω_{PQV}^{exit} and exit-P bus Ω_{P}^{exit} refer to the PQV bus and its associated P bus (or P buses), respectively, in the exit AVC strategy. According to the simulation results in Table 5, compared with scheme M1, the AVC control strategies will exit earlier under scheme M2 because the reactive power outputs of the

TABLE 5. Exit information of avc control strategies under schemes M1 and M2.

Scheme	Exit Point	Exit-PQV Bus Ω_{PQV}^{exit}	Exit-P Bus Ω_{P}^{exit}
M1	λ=0.0597	bus-B96	bus-B100
	λ=0.1133	bus-A12	bus-A32
	λ=0.3542	bus-A16	bus-A33, bus-A34
M2	λ=0.0189	bus-B96	bus-B100
	λ=0.0871	bus-A12	bus-A32
	λ=0.2808	bus-A16	bus-A33, bus-A34

corresponding P buses will reach the upper limit earlier in the process of load growth. The exit operations of AVC control strategies will further weaken the voltage supporting ability of the interconnected systems. Therefore, from the simulation results in Table 5, the following conclusion can be drawn from another perspective: whether the constant-voltage control of the boundary buses of tie-lines is considered or not has a substantial influence on the VSM of the interconnected systems.

D. CALCULATION CHARACTERISTICS OF THE PROPOSED DISTRIBUTED CPF ALGORITHM

The characteristics of the proposed distributed CPF algorithm in terms of computational accuracy, calculation speed, communication traffic and commercial confidentiality can be evaluated by comparing schemes M1 and M3. The only difference between schemes M1 and M3 is that scheme M1 adopts the distributed CPF algorithm that is proposed in this paper, while scheme M3 adopts the integrated CPF algorithm from reference [21]. The simulation results under schemes M1 and M3 are compared in Table 6.

TABLE 6. Comparison of the simulation results under schemes M1 and M3.

	M1	M3
VSM	0.3846	0.3846
Total Calculation Time (seconds)	2.5494	3.1842
Steps of Prediction-Correction	232	232
Dimensions of the Coefficient Matrices	65/184/6	255
Calculation Time of the Linear Equations	2574	858

First, the computational accuracy of the proposed distributed algorithm is analysed. According to the simulation results in Table 6, the calculated VSM and the number of prediction-correction steps that are required for increasing the initial load to the maximum load are the same under schemes M1 and M3. These results demonstrate that the proposed distributed CPF algorithm realizes very high computational accuracy and is highly consistent with the integrated algorithms in terms of not only the ultimate result but also the intermediate process. Theoretically, the proposed distributed algorithm is based on the strictly equivalent linear transformation; therefore, its calculation accuracy is equal to that of the integrated calculation.

Second, the calculation speeds of the proposed distributed algorithm and the integrated algorithm are compared and discussed. The total calculation times of the proposed distributed CPF algorithm and the integrated algorithm are

2.5494 and 3.1842 seconds, respectively. Therefore, the calculation speed is improved by nearly 20% with the proposed distributed algorithm. Both the prediction equation and the correction equation are linear equations whose computational dimensions can be represented by the dimensions of their coefficient matrices. Under scheme M2, the dimension of the integrated coefficient matrix is 255. In contrast, under scheme M1, the dimensions of the coefficient submatrices that correspond to subsystem-A, subsystem-B and the coupling zone are 65, 184 and 6, respectively. Therefore, the proposed distributed algorithm can decompose the process of solving the integrated linear equation into processes of solving three linear equations with smaller dimensions. According to Table 6, although the calculation times of the linear equations under scheme M1 are three times those under scheme M2, the total calculation time under scheme M1 is substantially less than that under scheme M2. Therefore, the reduction in the number of computational dimensions will substantially reduce the computational quantities. Moreover, in the proposed CPF algorithm, the decomposition-coordination method is adopted, and the related equations of each subsystem can be solved simultaneously and independently in a parallel manner. This will further increase the calculation speed. Compared with the integrated algorithm, the proposed distributed algorithm has an advantage in terms of the calculation speed, and this advantage will strengthen as the number of subsystems increases.

Finally, the characteristics of the proposed distributed algorithm in terms of the communication traffic and commercial confidentiality are discussed as follows:

(1) In each iteration, the regional server of each subsystem sends two square matrices and two vectors to the central coordinated server, the central sever send two vectors back to the regional servers, and no data need to be transferred among regional servers. This characteristic is unrelated to the scenarios of cases; it is universal.

(2) All the dimensions of the matrices and vectors that are transferred among servers are equal to the number of coupling variables. When the proposed distributed algorithm is adopted, the number of coupling variables is small; it typically ranges from a few to a dozen. For example, in this simulation case, the number of coupling variables is only 6; hence, the dimensions of the matrices and vectors that are transferred among servers are also only 6. Therefore, the proposed algorithm does not encounter difficulties in interactive communication.

(3) Because no commercial data are transferred among subsystems, the proposed distributed algorithm can also satisfy the requirements of commercial confidentiality for the internal data of regional power grid companies.

VI. CONCLUSIONS

This study proposes a novel CPF model and its corresponding distributed algorithm for interconnected systems under the influence of the electricity market. The proposed distributed CPF algorithm does not encounter difficulties with interactive communication, and it can satisfy the commercial confidentiality requirements for internal data of regional power grid companies. The results of case studies and a comparative analysis on a two-area interconnected system, which combines the IEEE 39-bus test system and the IEEE 118-bus test system, demonstrate the high performance of the proposed CPF model and the corresponding distributed algorithm. The following conclusions are drawn:

1) BPTC has a substantial influence on the CPF calculation for interconnected systems. Ignoring this influence will cause the calculated VSM to deviate far from reality. The derived nonlinear constraint equations of DTAP and the multi-balancing machine strategy have been proven effective in simulating the influence of BPTC on the CPF calculation.
2) In the proposed CPF model, the constant-voltage control behaviour of the boundary buses of the tie-lines is further considered to balance the partitioned reactive power and to avoid many reactive power exchanges among subsystems. The simulation results demonstrate that considering the constant-voltage control of boundary buses can not only ensure the reactive power balance among the regional subsystems but also improve the VSM of the entire interconnected system substantially.
3) The simulation results demonstrate that the proposed distributed CPF algorithm realizes very high computational accuracy and is highly consistent with the integrated algorithms in terms of not only the ultimate result but also the intermediate process. Moreover, according to the simulation comparisons, the proposed distributed CPF algorithm has an advantage in terms of the calculation efficiency compared with the integrated algorithms.

REFERENCES

[1] B. S. Adusumilli and B. K. Kumar, "Modified affine arithmetic based continuation power flow analysis for voltage stability assessment under uncertainty," *IET Gener., Transmiss. Distrib.*, vol. 12, no. 18, pp. 4225–4232, Oct. 2018.

[2] J. Zhao, Y. Wang, and P. Xu, "A comprehensive on-line voltage stability assessment method based on continuation power flow," in *Proc. Int. Conf. Sustain. Power Gener. Supply*, Nanjing, China, Apr. 2009, pp. 1–5.

[3] S. Palamarchuk, "Bilateral contract correction and cancellation in the competitive electricity markets," in *Proc. IEEE Bucharest PowerTech*, Bucharest, Romania, vol. 2, Jun./Jul. 2009, pp. 1–5.

[4] W. Yan, W. Cui, W.-J. Lee, J. Yu, and X. Zhao, "Pilot-bus-centered automatic voltage control with high penetration level of wind generation," *IEEE Trans. Ind. Appl.*, vol. 52, no. 3, pp. 1962–1969, May/Jun. 2016.

[5] A. Berizzi, C. Bovo, M. Delfanti, M. Merlo, and F. Tortello, "Singular value decomposition for an ORPF formulation in presence of SVR," in *Proc. IEEE Medit. Electrotech. Conf.*, Malaga, Spain, May 2006, pp. 968–972.

[6] H. Sun, Q. Guo, B. Zhang, W. Wu, and B. Wang, "An adaptive zone-division-based automatic voltage control system with applications in China," *IEEE Trans. Power Syst.*, vol. 28, no. 2, pp. 1816–1828, May 2013.

[7] H. Guo, M. Liu, and S. Lin, "Analysis of effects of secondary voltage control on static voltage stability," (in Chinese), *Autom. Electr. Power Syst.*, vol. 35, no. 6, pp. 20–24, Mar. 2011.

[8] J. Zhao, C. Zhou, and G. Chen, "A novel bus-type extended continuation power flow considering remote voltage control," in *Proc. IEEE PES General Meeting*, Vancouver, BC, Canada, Jul. 2013, pp. 1–5.

[9] H.-D. Chiang, A. J. Flueck, K. S. Shah, and N. Balu, "CPFLOW: A practical tool for tracing power system steady-state stationary behavior due to load and generation variations," *IEEE Trans. Power Syst.*, vol. 10, no. 2, pp. 623–634, May 1995.
[10] W. Yan, C. Ding, Z. Y. Ren, and W.-L. Lee, "A continuation power flow model of multi-area AC/DC interconnected bulk systems incorporating voltage source converter-based multi-terminal DC networks and its decoupling algorithm," *Energies*, vol. 12, no. 4, pp. 1–23, Feb. 2019.
[11] A. J. Flueck and J. R. Dondeti, "A new continuation power flow tool for investigating the nonlinear effects of transmission branch parameter variations," *IEEE Trans. Power Syst.*, vol. 15, no. 1, pp. 223–227, Feb. 2000.
[12] J.-Q. Zhao and B.-M. Zhang, "A study on the strategy for improving robustness of continuation power flow computation," in *Proc. CSEE*, Nov. 2005, vol. 25, no. 22, pp. 7–11.
[13] M. D. Amadou, H. Mehrjerdi, S. Lefebvre, M. Saad, and D. Asber, "Area voltage control analysis in transmission systems based on clustering technique," *IET Gener., Transmiss. Distrib.*, vol. 8, no. 12, pp. 2134–2143, Dec. 2014.
[14] Z. Ren, Y. Chen, S. Huang, and L. Zhang, "Searching severest VSM basing on CCPF among multiple dispatch centres," *IET Gener. Transm. Distrib.*, vol. 12, no. 6, pp. 1285–1293, Mar. 2018.
[15] L. Min and A. Abur, "Total transfer capability computation for multi-area power systems," *IEEE Trans. Power Syst.*, vol. 21, no. 3, pp. 1141–1147, Aug. 2006.
[16] H. Sun, Q. Guo, B. Zhang, Y. Guo, Z. Li, and J. Wang, "Master-slave-splitting based distributed global power flow method for integrated transmission and distribution analysis," *IEEE Trans. Smart Grid*, vol. 6, no. 3, pp. 1484–1492, May 2015.
[17] X. M. Su, C. X. Mao, and J. M. Lu, "Parallel load flow calculation of block bordered model," *Power Syst. Tech.*, vol. 26, no. 1, pp. 22–26, Jan. 2002 (In Chinese).
[18] S.-D. Chen and J.-F. Chen, "Fast load flow using multiprocessors," *Int. J. Electr. Power Energy Syst.*, vol. 22, no. 4, pp. 231–236, May 2000.
[19] Z. Haibo, Z. Boming, S. Hongbin, and A. Ran, "A new distributed power flow algorithm between multi-control-centers based on asynchronous iteration," in *Int. Conf. Power Syst. Technol.*, Chongqing, China, Oct. 2006, pp. 1–7.
[20] C. A. Canizares and F. L. Alvarado, "Point of collapse and continuation methods for large AC/DC systems," *IEEE Trans. Power Syst.*, vol. 8, no. 1, pp. 1–8, Feb. 1993.
[21] V. Ajjarapu and C. Christy, "The continuation power flow: A tool for steady state voltage stability analysis," *IEEE Trans. Power Syst.*, vol. 7, no. 1, pp. 416–423, Feb. 1992.
[22] X. Zhang, R. H. Byrd, and R. B. Schnabel, "Parallel methods for solving nonlinear block bordered systems of equations," *SIAM J. Sci. Statist. Comput.*, vol. 13, no. 4, pp. 841–859, Nov. 1992.
[23] Y. Gao, Z. Wang, and H. Liang, "Available transfer capability calculation with large offshore wind farms connected by VSC-HVDC," in *Proc. IEEE PES Innov. Smart Grid Technol.*, Tianjin, China, May 2012, pp. 1–6.